Miles, R., Glerum, M., Boyer, H., Walker, J., Dutcher, C., & Bzdek, B. (2019). Surface Tensions of Picoliter Droplets with Sub-Millisecond Surface Age. *Journal of Physical Chemistry A*, *123*(13), 3021-3029. https://doi.org/10.1021/acs.jpca.9b00903

Surface Tensions of Picoliter Droplets with Sub-Millisecond Surface Age

Rachael E. H. Miles[1], Michael W. J. Glerum[1], Hallie C. Boyer[2,†], Jim S. Walker[1], Cari S. Dutcher[2], and Bryan R. Bzdek[1,]*

[1]School of Chemistry, University of Bristol, Cantock's Close, Bristol, BS8 1TS, United Kingdom

[2]Department of Mechanical Engineering, University of Minnesota, Twin Cities, Minneapolis, Minnesota 55455, United States

ABSTRACT

Aerosols are key components of the atmosphere and play important roles in many industrial processes. Because aerosol particles have high surface-to-volume ratios, their surface properties are especially important. However, direct measurement of the surface properties of aerosol particles is challenging. In this work, we describe an approach to measure the surface tension of picoliter volume droplets with surface age <1 ms by resolving their dynamic oscillations in shape immediately after ejection from a microdroplet dispenser. Droplet shape oscillations are monitored by highly time resolved (500 ns) stroboscopic imaging, and droplet surface tension is accurately retrieved across a wide range of droplet sizes (10-25 μm radius) and surface ages (down to ~100 μs). The approach is validated for droplets containing sodium chloride, glutaric acid, and water, which all show no variation in surface tension with surface age. Experimental results from the microdroplet dispenser approach are compared to complementary surface tension measurements of 5-10 μm radius droplets with aged surfaces using a holographic optical tweezers approach and

predictions of surface tension using a statistical thermodynamic model. These approaches combined will allow investigation of droplet surface tension across a wide range of droplet sizes, compositions, and surface ages.

INTRODUCTION

The surface properties of aerosol particles are relevant to a wide range of contexts, spanning environmental science to industrial processes. The effects of aerosols on clouds and climate is the largest uncertainty in anthropogenic radiative forcing estimates,[1] and uncertainty in what fraction of atmospheric particles ultimately serve as cloud droplets is an important contributor. The Köhler equation describes the critical supersaturation in relative humidity required to successfully grow a cloud droplet and is highly dependent on a particle's surface tension, which determines the height of the barrier in supersaturation to cloud droplet activation.[2] Therefore, surface tension influences the fraction of atmospheric particles that ultimately grow into cloud droplets.[3,4] Models implicitly assume the surface tension at cloud droplet activation is equivalent to that of pure water, but this assumption has not been rigorously tested. Modification of the surface tension value to one consistent with those of surfactant solutions could affect radiative forcing by as much as 1.1 $W \cdot m^{-2}$.[5] Mounting evidence indicates atmospheric particles contain surface active and other molecules that lower the surface tension.[6–12] Surface composition also impacts the transport of molecules across the particle-air interface. For instance, long-chain acids and alcohols can form condensed films on droplets and impede water evaporation,[13,14] which has relevance to the timescales for these droplets to reach thermodynamic equilibrium with their surroundings. Moreover, the droplet-air interface is known to be reactive,[15–17] highlighting the importance of resolving interfacial composition.

Despite the importance of the particle surface, a direct understanding of surface properties is very challenging for several reasons.[18] First, individual aerosol particles, due to their small size, have very little mass, so collection of large numbers of particles is required to make a macroscopic solution measurement of surface tension.[6,7,12] Collection is made especially challenging because aerosols are highly dynamic systems that rapidly respond to environmental conditions. There are also dispersions in size and composition, so collected aerosol surface properties represent average properties across a population rather than the properties of an individual particle. Second, it is not always clear whether macroscopic solution measurements directly translate to microscopic particles owing to the high surface-to-volume ratios inherent to aerosol. As the surface-to-volume ratio increases (i.e. droplet size decreases), a larger fraction of surface active molecules in the droplet must partition to the surface. The result is that the bulk concentration can be reduced relative to a comparable macroscopic solution, and surface tension is higher than in the corresponding macroscopic solution.[19–23] Third, aerosols can access compositions and phases inaccessible in macroscopic solutions (e.g. supersaturated solute states, glassy phases). Although approaches exist to predict surface tension beyond the bulk solubility limit, limited surface tension measurements in this concentration regime have been reported.[24,25] As a consequence of these challenges, direct measurements of droplet surface tension are required to validate model predictions in supersaturated solute concentration regimes and to quantify the partitioning behavior of surface active molecules.

Broadly, two approaches exist to directly measure the surface tension of individual picoliter aerosol droplets. One approach uses Atomic Force Microscopy to quantify the surface tension of micron and submicron particles deposited on a substrate.[26,27] The approach measures the retention force between a nanoneedle and liquid droplet, which can then be related to the surface tension.

69 The benefit of this approach is the ability to access particle sizes of atmospheric interest. The
70 drawbacks are that particles must be collected onto a substrate and that particle viscosity can also
71 affect the retrieved force profile, complicating measurement interpretation.[27] Another set of
72 approaches is defined by monitoring spontaneous or induced oscillations in an airborne droplet.[28–
73 30] For example, we have previously developed an approach to measure directly picoliter droplet
74 surface tension through coalescence of two optically trapped droplets.[24,25,31] Others have examined
75 spontaneous oscillations in an optically trapped droplet.[32] A benefit of stably trapping a droplet for
76 long time periods is that equilibrium surface composition is usually achieved. Other methods to
77 investigate the surface properties of picoliter droplets study their oscillations shortly after ejection
78 from a microdroplet dispenser.[33–38] A benefit of studying freshly formed surfaces is that dynamic
79 partitioning processes can be resolved. Dynamic processes at the droplet interface may affect an
80 atmospheric particle's activity as a cloud condensation nucleus.[12]

81 In this paper, we describe an approach to resolve the surface tension of 10-25 μm radius
82 picoliter droplets with surface age <1 ms by reproducible droplet ejection from a microdroplet
83 dispenser. The novel aspect relative to previously reported approaches[33–38] is that we explore a
84 much larger parameter space, investigating a wider range of particle size, oscillation time, and
85 chemical composition than previous studies. In addition, we examine in detail measurement-to-
86 measurement reproducibility across all parameters, with an aim to develop this approach into a
87 robust platform to investigate the dynamic surface tension of fresh droplet surfaces across a wide
88 size range. The systems investigated with the microdroplet dispenser approach (water, glutaric
89 acid, sodium chloride, and various mixtures) are compared to surface tension measurements made
90 on aged surfaces of 5-10 μm radius droplets using holographic optical tweezers[24,25] and to
91 statistical thermodynamic model predictions.[25] Combined, the fresh surface and aged surface

approaches allow surface tension measurement across different timescales, length scales, and concentration regimes, and will permit robust investigation of time dependent and equilibrium surface tension measurements for picoliter volume aerosol droplets.

METHODS

Two complementary experimental approaches were utilized to measure the surface tensions of picoliter volume droplets. Both approaches rely on excitation of droplet oscillatory modes to retrieve surface tension. Although the details of each approach will be further discussed, the salient differences in these approaches are illustrated pictorially in Fig. 1. The first approach utilizes microdroplet dispensers to produce droplets with surface ages <1 ms (Fig. 1a). For comparison, the shortest timescales accessible to bulk solution approaches that measure dynamic surface tension (e.g. bubble pressure tensiometry) are typically ~10 ms. The second approach utilizes holographic optical tweezers to examine droplets that have been allowed several tens of seconds for their surfaces to age, usually reaching their equilibrium surface composition before measurement (Fig. 1b). These two approaches are complementary, allowing comparison of fresh and aged droplet surface compositions.

As shown in Fig. 1, both approaches retrieve surface tension through examination of damped shape oscillations that are excited either by pulsing a droplet from a dispenser (Fig. 1a) or by coalescence of two droplets (Fig. 1b). The frequency of these oscillations gives the droplet surface tension, σ:[28,30]

$$\sigma = \frac{a^3 \rho \omega_l^2}{l(l-1)(l+2)} \qquad (1)$$

where a is the droplet radius, ρ is the droplet density, and ω_l is the angular oscillation frequency of a given mode order l. In these studies, only l=2 modes were used to retrieve droplet surface tension.

Fresh droplet surface measurements. As shown in Fig. 1a the surface tension of newly formed droplets (i.e. droplets with surface ages <1 ms) was studied through analysis of the rapid surface oscillations apparent in droplets produced by a microdroplet dispenser. The experimental approach is illustrated in Fig. 2. All measurements were performed at room temperature. A repeating voltage pulse was applied to a piezo microdroplet dispenser (MicroFab MJ-ABP-01) filled with a desired solution in order to dispense at 10 Hz a stream of uniform individual droplets. The size of a dispensed droplet was controlled by the amplitude, duration, and shape of the voltage pulse, and typically ranged from 10 to 25 μm radius. Ejection from the dispenser excites surface oscillatory modes in the droplet, which were monitored using stroboscopic imaging. A white light LED (Nichia NSPW500GS-K1) was pulsed for 500 ns at a user-controlled delay time after the voltage pulse that dispensed the droplet. As the LED delay time was incremented forwards, the temporal evolution in droplet shape was imaged with a camera (JAI GO-2400M-USB) mounted on a microscope objective (Optem 28-21-11, M Plan APO 20X). Custom written software (LabVIEW) automatically identified the droplet in the 8-bit greyscale image and calculated the size and aspect ratio. The droplet was identified by comparing the value of each pixel in the image against a threshold value. Sufficiently large groupings of darker pixels were identified as a droplet and isolated from the background. A box was superimposed around the image of the droplet to calculate the height and width, in pixels, as shown in Fig. 2b. The droplet aspect ratio (a_y/a_x) was determined as the ratio of the height (a_y) to the width (a_x), and the droplet radius was calculated from the width once it relaxed to spherical shape ($a_y/a_x=1$). The droplet radius was converted from pixels to SI units by multiplying the number of pixels by their measured length scale. The pixel length scale (typically 0.172 μm·pixel^{-1}) was calibrated before each measurement using a graticule. Due to the short measurement timescale, solvent evaporation from the droplet (e.g. water loss) is

minimal. Therefore, the droplet radius retrieved at the end of the oscillation is equivalent to the size of the droplet at the start of the measurement. Calibration measurements using a water droplet were performed before each salt solution experiment to ensure the correct threshold limit had been set on the camera, giving accurate determination of the droplet size and extraction of the correct water surface tension (73 $mN \cdot m^{-1}$). The stroboscopic imaging approach relies on highly reproducible production of dispensed droplets. In the measurements, continuous imaging at a fixed time delay following droplet ejection produced a static droplet image, indicating stability in both size and velocity from one dispensed droplet to the next. In a typical experiment to characterize a single droplet's progression in shape, over 500 different but identical droplet generation events were studied. The stability of droplet production by this approach has been noted previously.[39–41]

Upon droplet generation, multiple surface oscillatory mode orders (e.g. $l = 2$, $l = 3$, etc.) are observed. Because higher order ($l > 2$) modes damp out quickly, droplet aspect ratios were retrieved only after these higher order modes relaxed (typically ~10-60 μs depending on droplet size and oscillatory energy). Droplet aspect ratios were retrieved from each individual image as the strobe delay time was systematically increased in intervals of between 0.1 – 1 μs. As shown in Fig. 2c, droplet aspect ratios were plotted against the strobe delay time, resulting in a characteristic damped oscillator. The angular oscillation frequency was retrieved by applying the Fast Fourier Transform (FFT) to the plot of aspect ratio against delay time. As illustrated in Fig. 2d, the peak position of the oscillatory frequency was retrieved by fitting the power spectrum to a Lorentzian line shape. An alternative, equivalent approach is to fit the experimental data to a damped oscillator equation. Note that the linewidth of the Lorentzian also provides information about the droplet viscosity, which for all studied droplets was ~1-5 mPa·s. The droplet viscosity does not substantially affect the frequency of the droplet oscillations, instead only impacting the rate at

which the oscillations decay away. The uncertainties in the peak oscillatory frequency (arising from the goodness of fit between the FFT data and the Lorentzian line shape) and in the droplet radius (assumed to be the greater of either the pixel length scale or the standard deviation in droplet radii measured from successive images) were propagated in the calculation of the surface tension. The uncertainty in the droplet radius is the dominant factor governing the uncertainty in the extracted surface tension. As will be demonstrated later, this approach allows retrieval of droplet surface tension with a typical uncertainty of around ±2 $mN \cdot m^{-1}$.

Aged droplet surface measurement. As illustrated in Fig 1b, the holographic optical tweezers approach allows measurement of droplet surface tensions where the droplet surfaces have been provided time to age and potentially reach their equilibrium state. This approach has been described in detail previously.[24,25,31,42] Briefly, droplets 5-10 μm radius produced from a medical nebulizer (Omron NE U22) were captured in two optical traps formed by dynamically shaping the phase front of a 532 nm continuous wave laser (Laser Quantum, Opus 3W) with a spatial light modulator (SLM, Hamamatsu, X10468). The laser beam was expanded to fill the SLM display and was conjugated to the back focal plane of a high numerical aperture microscope objective (Olympus ACH, 100×/1.25, oil). The separation of the optical traps was controlled by a pre-calculated sequence of kinoforms, and the rate at which the kinoforms were changed was user-controlled. Once the trap separation was sufficiently small, the droplets coalesced into one composite droplet. The droplet position was monitored with a camera (Dalsa Genie HM 640, CMOS) and illuminated with a high powered LED (Thorlabs, 470 nm). Inelastically backscattered (Raman) light was directed to a 0.5 m focal length spectrograph (Princeton Instruments, Acton Spectra Pro SP-2500), dispersed by a 1200 $grooves \cdot mm^{-1}$ grating onto a Peltier cooled CCD. The Raman spectrum from a spherical droplet consists of a broad spontaneous Raman band with

184 stimulated signal at wavelengths commensurate with whispering gallery modes.[43] From the
185 stimulated Raman signal, the composite droplet radius, refractive index, and wavelength
186 dispersion can be determined with accuracies better than 2 nm, 0.0005, and 3×10^{-8} cm,
187 respectively.[44] Elastic backscattered light was collected using a silicon photodetector (Thorlabs,
188 DET 110) and recorded with a low-load, 12 bit analog-to-digital converter resolution, 2.5 $GS\cdot s^{-1}$
189 sample rate oscilloscope (LeCroy, HDO 6034-MS). Collection of backscattered light was triggered
190 by an increase in signal due to coalescence. Droplet shape oscillations were resolved from the
191 time-dependent changes in elastic backscattered light intensity.[24,31] Surface tensions retrieved by
192 this approach are typically accurate to ±1 $mN\cdot m^{-1}$.[24] As shown in Fig. 1b, after trapping the two
193 precursor droplets, it typically requires several tens of seconds to initiate coalescence, allowing
194 sufficient time for the droplet surfaces to age and reach their equilibrium state. Once coalescence
195 is initiated, the damped oscillations occur on timescales of 10-100 μs, and it is at this time that
196 droplet surface tension is retrieved. Although coalescence decreases the total surface area of the
197 droplets (two smaller droplets forming one larger droplet with lower total surface area), it is
198 assumed that the small change in composite droplet surface area does not substantially remove the
199 droplet surface composition from equilibrium for the systems studied here.

200 *Statistical thermodynamic model.* Experimentally measured droplet surface tensions were
201 compared to a statistical thermodynamic model. This model has been described in detail previously
202 and is only summarized here.[25] Using adsorption isotherms at the interface and statistical
203 mechanics, a previously developed surface tension model by Boyer et al. successfully treated
204 multicomponent aqueous solutions.[25] The model worked equally well for mixtures containing
205 water-soluble organics, electrolytes, and both organics and electrolytes. The theoretical framework
206 extended a prior binary model by Wexler and Dutcher.[45] In the binary model development, the

surface is populated with water molecules, which represent the adsorption sites. Solutes adsorb to the surface and displace *r* water molecules, where *r* is a model parameter associated with the size of the solute molecule. The resulting expression is

$$\sigma = \sigma_w + \frac{kT}{rS_w} ln\left(\frac{1 - Ka_s}{1 - Ka_s(1 - C)}\right) \quad (2)$$

where σ_w is the surface tension of pure water, *k* is Boltzmann's constant, *T* is temperature, S_w is the projected area of one water molecule (0.01 nm^2), and a_s is the solute activity. The remaining model parameters are *K*, which is a bulk energy term, and *C*, which represents the equilibrium surface-bulk partitioning of solute molecules. For inorganic electrolytes, *r* is a negative value, indicating that water molecules are promoted to the surface, rather than displaced from the surface.

In the ternary model, two arbitrary solutes compete for interfacial sorption sites with equal probability. Each model parameter (*r*, *K*, and *C*) is decoupled so the two solutes are assigned parameters from the binary model. The resulting system of equations and computational methods, as well as model extension to an arbitrary number of solutes, are discussed in Boyer et al.[25] Multicomponent model predictions do not require additional parameters but are instead produced from the previously known binary treatments and ternary model expressions. Therefore, when there are known parameters that work well for binary data, surface tensions at any solute ratio are available. Single solute data are more commonly reported in the literature than mixture data. This model agrees well with ternary mixture data when they are available, as well as provides predictions where data are not available.[25]

RESULTS AND DISCUSSION

To characterize the range and reproducibility of the fresh droplet surface approach, the surface tensions of pure water droplets, glutaric acid-water droplets, and sodium chloride-water

droplets were investigated as a function of droplet size and time after ejection from the microdroplet dispenser. Figure 3a shows the droplet aspect ratio plotted against delay time for a 24 μm radius pure water droplet. In this plot, time t=0 s is defined as the moment the voltage pulse is applied to the microdroplet dispenser, with subsequent time points determined by the user-imposed delay between application of the voltage pulse and the stroboscopic imaging. Aspect ratios are only collected after ~150 μs because at earlier time points the droplet has either not yet separated from the liquid jet produced by the dispenser, or, immediately after separation, higher order surface oscillations are operative and complicate retrieval of droplet aspect ratios. As expected, droplet shape proceeds through damped oscillations that relax after ~550 μs.

The surface tension retrieved using the droplet oscillation method is the average of the droplet surface tension during the time period over which the aspect ratio data are Fast Fourier transformed. As the droplet undergoes several periods of oscillation before the l = 2 oscillatory mode relaxes, it is possible to systematically shorten the aspect ratio data set that is Fast Fourier transformed by removing early data points. This process provides information about any dynamic processes that may be occurring during oscillation which would lead to a change in surface tension (e.g. diffusion of surface active molecules to the droplet-air interface), as well as providing guidance on the quality of aspect ratio data required for accurate surface tension retrieval (e.g. number of shape oscillations that must be monitored). Figure 3b shows the Lorentzian line shapes fitted to the FFT of the droplet aspect ratio plot in Fig. 3a, with each color trace showing the result when only aspect ratio data to the right of the corresponding colored dotted line in Fig. 3a are included in the FFT. For example, the red trace in Fig. 3b shows the Lorentzian fit to the FFT of the aspect ratio plot from 208 μs to 608 μs, whereas the purple trace in Fig. 3b shows the Lorentzian fit to the FFT of the aspect ratio plot from 415 μs to 608 μs for the same droplet. If diffusion or

adsorption processes are operative near the surface during the timescale of droplet shape oscillation, one would expect the frequency retrieved from the FFT and the corresponding surface tension to change as the early time points of the aspect ratio plot are removed. In Fig. 3b, although the magnitude of the peak reduces as the number of data points analyzed decreases, the central frequency remains roughly constant.

Figure 3c shows retrieved water droplet surface tensions for different portions of the aspect ratio dataset. The x-axis reports the droplet surface age. In this work, creation of a new droplet surface is considered complete when the droplet separates itself from the jet emanating from the microdroplet dispenser (pinch off time). This moment is assigned a surface age of t=0 s and all calculations of surface age are referenced to this point. Voltage pulses to the dispenser that produce only a single droplet per pulse (resulting in a dispenser meniscus age of 100 ms for a 10 Hz dispensing frequency) and voltage pulses producing a stream of up to six droplets per pulse (meaning the meniscus was refreshed every 50–100 μs) were examined in this study. No differences were found in the behavior of the two types of droplets when the surface age was defined relative to the pinch off time. Therefore, we ignore any consideration of the age of the dispenser meniscus when discussing the droplet surface age. In Fig. 3c the x-value uncertainty bar denotes the surface age range over which the aspect ratio data were Fast Fourier transformed to give the plotted surface tension value. Regardless of the surface age range included in the FFT, the droplet surface tension was always within error of the expected value of 73 $mN \cdot m^{-1}$. Figure 3 therefore demonstrates we can accurately retrieve the surface tension of a water droplet to within 2 $mN \cdot m^{-1}$ and that only a few shape oscillations are required to accurately retrieve surface tension. In the results that follow, reported surface tension values are calculated from Fast Fourier

Transforming the maximum number of droplet oscillations possible to minimize the uncertainty in the retrieved oscillation frequency.

We now explore size and time dependencies of surface tension for droplets containing either glutaric acid and water, or sodium chloride and water. These systems are chosen because they give different trends in surface tension with increasing concentration (glutaric acid reduces surface tension, whereas sodium chloride increases surface tension) and they are model compounds for atmospheric aerosols like organic matter (glutaric acid) and sea salt (sodium chloride). Figure 4a shows the droplet aspect ratio for a 21 μm radius glutaric acid-water droplet containing 0.010 solute mole fraction. Similar to Fig. 3a, the aspect ratio data were systematically shortened to evaluate the surface age dependence of the droplet's surface tension. Figure 4b shows that no obvious time dependence to surface tension is observed, consistent with expectations as glutaric acid is not a surfactant. Figure 4c shows the retrieved surface tensions for sodium chloride-water (0.062 solute mole fraction) and glutaric acid-water (0.090 solute mole fraction) droplets as a function of droplet radius. For each system, individual data points are produced from the same initial solution (i.e. same solute concentration). Droplet size was changed by modifying the voltage pulse applied to the microdroplet dispenser. As expected, the sodium chloride-water and glutaric acid-water droplets have very different surface tensions (77 $mN \cdot m^{-1}$ for sodium chloride-water droplets, 54 $mN \cdot m^{-1}$ for glutaric acid-water droplets) that are clearly resolvable. There are also no size dependencies to the surface tension measurements. A size dependent surface tension would be expected only if surface-bulk partitioning were operative for these systems, as the surface-to-volume ratios would change with droplet size. A smaller droplet has a larger surface-to-volume ratio, potentially requiring a larger fraction of total surface active material in the droplet to partition to the surface.[20,23] Although glutaric acid has some surface propensity, it is not a surfactant, and

298 we do not observe any size dependence. These results are also consistent with equilibrium surface
299 tension measurements previously reported using the holographic optical tweezers approach.[24,25]
300 The above discussion demonstrates the microdroplet dispenser approach reproducibly
301 provides accurate surface tension measurements across a range of droplet radii spanning ~10 μm
302 to 25 μm. We next investigate the dependencies of surface tension on solute identity across a range
303 of compositions and concentrations, examining binary mixtures of glutaric acid-water and sodium
304 chloride-water, as well as several ternary sodium chloride-glutaric acid-water mass mixtures. The
305 experimental results using the fresh droplet surface approach are compared to aged surface
306 measurements using holographic optical tweezers and statistical thermodynamic model
307 predictions. These results are presented in Fig. 5. Closed circles represent the microdroplet
308 dispenser (fresh droplet surface) approach, open triangles represent holographic optical tweezers
309 (aged droplet surface) approach, and solid lines represent model predictions. The uncertainty bars
310 associated with each data point correspond to an average of at least three separate measurements,
311 with the fresh droplet surface measurements also including the uncertainty in surface tension
312 arising from the error in droplet radius. Extensive concentration dependent measurements were
313 performed for binary sodium chloride-water (blue) and glutaric acid-water (red) systems using the
314 microdroplet dispenser approach. The binary model parameters were identified by fitting available
315 bulk solution data measured by Wilhelmy plate.[46] Surface tension predictions in the supersaturated
316 regime accessible with optical tweezers were successfully predicted with the model for both NaCl
317 and glutaric acid binary solutions, as shown in previous work.[25] Fresh droplet surface
318 measurements for the sodium chloride-water system show excellent agreement with previously
319 published holographic optical tweezers measurements and statistical thermodynamic model
320 predictions, with all measurements and predictions within ~2.5 $mN \cdot m^{-1}$.[24,25] Similarly, good

agreement is observed among all approaches for the glutaric acid-water system, with similar levels of agreement.

Several different mass mixtures were also examined. For a given solute mass ratio, only one concentration was studied experimentally with the microdroplet dispenser approach. However, more extensive, concentration dependent measurements were performed using the holographic optical tweezers approach, maintaining a constant solute mass ratio throughout measurements while changing the total concentration (sum of mole fractions). The model predictions span a concentration range from infinitely dilute to far past the solubility and measurement limits. The parameters applied to the mixture model originate from the binary model, requiring no further parametrization for ternary solutions. The model predicts surface tension by allowing the organic and electrolytes to compete for surface adsorption sites with equal probability. For the 1:1 mass ratio sodium chloride:glutaric acid system, for which holographic optical tweezers measurements and model predictions were previously reported,[25] the microdroplet dispenser measurements agree quantitatively with the holographic optical tweezers aged surface measurements and match closely with model predictions. We also report both fresh and aged droplet surface measurements for two previously unpublished systems: 4:1 mass ratio sodium chloride:glutaric acid and 16:1 mass ratio sodium chloride:glutaric acid. The agreement between measurements and the model prediction is remarkable considering the very low glutaric acid fraction in the system as well as the relatively small (<5 mN·m^{-1}) differences in surface tension for these two systems. The slight (~5 mN·m^{-1}) disagreement between the holographic optical tweezers measurements and model predictions at very low solute mole fractions for the 4:1 mass ratio system is because at such low concentrations, the water activity is very large and stable optical trapping of droplets is more challenging.

343 The close agreement between the fresh surface (microdroplet dispenser) and aged surface
344 (holographic optical tweezers) measurements highlights the rapid equilibration of droplet surfaces
345 at sub-millisecond timescales. The uniformity in surface tension across a wide range of length
346 scales is also notable. The holographic optical tweezers approach measures a smaller droplet size
347 range (5-10 μm radius) than the microdroplet dispenser approach (10-25 μm radius). The model
348 treats the droplet as a surface and therefore does not consider size dependent effects. The
349 agreement among all approaches indicates that, at least for these non-surfactant-containing
350 systems and droplet sizes, bulk predictions or measurements of surface tension are appropriate.
351 However, it is worth highlighting that the holographic optical tweezers approach, owing to its
352 ability to let droplets equilibrate over time to ambient conditions, can access supersaturated solute
353 states well beyond the solubility limit. Such measurements permit testing of models in previously
354 untestable concentration regimes. In Fig. 5, the sodium chloride-water droplets beyond 0.113
355 solute mole fraction and the glutaric acid-water droplets beyond 0.147 solute mole fraction are in
356 the supersaturated solute regime and match well with model predictions. For the microdroplet
357 dispenser approach, the timescales for stable droplet formation and oscillation are too short to
358 allow sufficient mass transfer (e.g. water evaporation) to reach such supersaturated solute states.
359 However, the microdroplet dispenser approach can more easily study very dilute systems
360 (including pure water, Fig. 3) which is significantly more challenging in the holographic optical
361 tweezers experiments, as the water activity is too high to stably trap a droplet. In short, although
362 all three approaches ultimately give the same result, they are in fact highly complementary,
363 measuring or predicting surface tensions across very different timescales (fresh vs. aged surfaces),
364 length scales (5 μm radius up to bulk systems), and concentration regimes (infinitely dilute to
365 supersaturated solute states).

CONCLUSIONS

This work describes an approach to measure the surface composition of picoliter volume droplets with surface age <1 ms. Droplets are ejected from a microdroplet dispenser and imaged stroboscopically to retrieve the characteristic shape oscillations that describe their surface tension. This approach is characterized for pure water droplets, binary droplets containing glutaric acid and water or sodium chloride and water, and ternary sodium chloride-glutaric acid-water droplets at different solute mass ratios. For the systems studied here, surface tension is accurately retrieved across a range of droplet radii and droplet surface ages. The fresh surface measurements collected using the microdroplet dispenser approach are compared to aged surface measurements collected using a holographic optical tweezers approach, as well as to statistical thermodynamic model predictions. Excellent agreement is observed among the different methods. The approaches are highly complementary, spanning different timescales (fresh vs. aged surfaces), length scales (5 μm radius up to bulk predictions), and concentration regimes (infinitely dilute to supersaturated solute states). Future work will investigate more complicated surfactant containing systems, where diffusion rates are slower and surface-bulk partitioning more significant. Previous preliminary investigations have indicated that the timescales of surfactant partitioning to the surface are of similar magnitude to the droplet oscillation period.[33,34,36–38] Such experiments will identify timescales and mechanisms for molecular partitioning in picoliter droplets relevant to atmospheric and industrial contexts.

AUTHOR INFORMATION

Corresponding Author

*Phone: +44 (0)117 331 8387. Electronic mail: b.bzdek@bristol.ac.uk

Present Addresses

†H. C. B.: Center for Atmospheric Particle Studies, Carnegie Mellon University, Pittsburgh, Pennsylvania 15213

ACKNOWLEDGMENTS

B.R.B. acknowledges support from the Natural Environment Research Council (NERC) through Grant No. NE/P018459/1. R.E.H.M. and J.S.W. acknowledge support from the Engineering and Physical Sciences Research Council (EPSRC) through Grant No. EP/N025245/1. H.C.B. and C.S.D. acknowledge support from the National Science Foundation (NSF) under Grant No. 1554936; the College of Science and Engineering Characterization Facility, University of Minnesota, which receives funding from the NSF through the UMN MRSEC under Award DMR-1420013; and support for H.C.B through a National Science Foundation Graduate Research Fellowship through NSF Grant No. 00039202. Ivo Videnov is acknowledged for holographic optical tweezers measurements on the 4:1 and 16:1 sodium chloride:glutaric acid mass mixtures. Data are available at the University of Bristol data repository, data.bris, at https://doi.org/10.5523/bris.2iw9uz9kakurk2brsd3koror01.

REFERENCES

(1) IPCC. *Climate Change 2013 : The Physical Science Basis : Working Group I Contribution to the Fifth Assessment Report of the Intergovernmental Panel on Climate Change*; Stocker, T. F., Qin, D., Plattner, G.-K., Tignor, M., Allen, S. K., Boschung, J., Nauels, A., Xia, Y., Bex, V., Midgley, P. M., Eds.; Cambridge University Press: Cambridge, 2013.

(2) Köhler, H. The Nucleus in and the Growth of Hygroscopic Droplets. *Trans. Faraday Soc.* **1936**, *32*, 1152–1161.

(3) Ruehl, C. R.; Davies, J. F.; Wilson, K. R. An Interfacial Mechanism for Cloud Droplet Formation on Organic Aerosols. *Science* **2016**, *351*, 1447–1450.

(4) Ovadnevaite, J.; Zuend, A.; Laaksonen, A.; Sanchez, K. J.; Roberts, G.; Ceburnis, D.; Decesari, S.; Rinaldi, M.; Hodas, N.; Facchini, M. C.; et al. Surface Tension Prevails over

Solute Effect in Organic-Influenced Cloud Droplet Activation. *Nature* **2017**, *546*, 637–641.
(5) Prisle, N. L.; Asmi, A.; Topping, D.; Partanen, A. I.; Romakkaniemi, S.; Dal Maso, M.; Kulmala, M.; Laaksonen, A.; Lehtinen, K. E. J.; McFiggans, G.; et al. Surfactant Effects in Global Simulations of Cloud Droplet Activation. *Geophys. Res. Lett.* **2012**, *39*, L05802, doi: 10.1029/2011GL050467.
(6) Gérard, V.; Nozière, B.; Baduel, C.; Fine, L.; Frossard, A. A.; Cohen, R. C. Anionic, Cationic, and Nonionic Surfactants in Atmospheric Aerosols from the Baltic Coast at Askö, Sweden: Implications for Cloud Droplet Activation. *Environ. Sci. Technol.* **2016**, *50*, 2974–2982.
(7) Facchini, M. C.; Mircea, M.; Fuzzi, S.; Charlson, R. J. Cloud Albedo Enhancement by Surface-Active Organic Solutes in Growing Droplets. *Nature* **1999**, *401*, 257–259.
(8) Sareen, N.; Schwier, A. N.; Lathem, T. L.; Nenes, A.; McNeill, V. F. Surfactants from the Gas Phase May Promote Cloud Droplet Formation. *Proc. Natl. Acad. Sci.* **2013**, *110*, 2723–2728.
(9) McNeill, V. F.; Sareen, N.; Schwier, A. N. Surface-Active Organics in Atmospheric Aerosols. In *Atmospheric and Aerosol Chemistry*; Springer, Berlin, Heidelberg, 2013; pp 201–259.
(10) Kroflič, A.; Frka, S.; Simmel, M.; Wex, H.; Grgić, I. Size-Resolved Surface-Active Substances of Atmospheric Aerosol: Reconsideration of the Impact on Cloud Droplet Formation. *Environ. Sci. Technol.* **2018**, *52*, 9179–9187.
(11) Frka, S.; Dautović, J.; Kozarac, Z.; Ćosović, B.; Hoffer, A.; Kiss, G. Surface-Active Substances in Atmospheric Aerosol: An Electrochemical Approach. *Tellus, Ser. B Chem. Phys. Meteorol.* **2012**, *64*, 18490, doi: 10.3402/tellusb.v64i0.18490.
(12) Nozière, B.; Baduel, C.; Jaffrezo, J. L. The Dynamic Surface Tension of Atmospheric Aerosol Surfactants Reveals New Aspects of Cloud Activation. *Nat. Commun.* **2014**, *5*, 3335, doi: 10.1038/ncomms4335.
(13) Davies, J. F.; Miles, R. E. H.; Haddrell, A. E.; Reid, J. P. Influence of Organic Films on the Evaporation and Condensation of Water in Aerosol. *Proc. Natl. Acad. Sci.* **2013**, *110*, 8807–8812.
(14) Ruehl, C. R.; Wilson, K. R. Surface Organic Monolayers Control the Hygroscopic Growth of Submicrometer Particles at High Relative Humidity. *J. Phys. Chem. A* **2014**, *118*, 3952–3966.
(15) Knipping, E. M.; Lakin, M. J.; Foster, K. L.; Jungwirth, P.; Tobias, D. J.; Gerber, R. B.; Dabdub, D.; Finlayson-Pitts, B. J. Ion-Enhanced Interfacial Chemistry on Aqueous NaCl Aerosols. *Science* **2000**, *288*, 301–306.
(16) Rossignol, S.; Tinel, L.; Bianco, A.; Passananti, M.; Brigante, M.; Donaldson, D. J.; George, C. Atmospheric Photochemistry at a Fatty Acid-Coated Air-Water Interface. *Science* **2016**, *353*, 699–702.
(17) Griffith, E. C.; Carpenter, B. K.; Shoemaker, R. K.; Vaida, V. Photochemistry of Aqueous Pyruvic Acid. *Proc. Natl. Acad. Sci.* **2013**, *110*, 11714–11719.
(18) Bzdek, B. R.; Reid, J. P. Perspective: Aerosol Microphysics: From Molecules to the Chemical Physics of Aerosols. *J. Chem. Phys.* **2017**, *147*, 220901.
(19) Li, Z.; Williams, A. L.; Rood, M. J. Influence of Soluble Surfactant Properties on the Activation of Aerosol Particles Containing Inorganic Solute. *J. Atmos. Sci.* **1998**, *55*, 1859–1866.
(20) Sorjamaa, R.; Raatikainen, T.; Laaksonen, A. The Role of Surfactants in Köhler Theory

Reconsidered. *Atmos. Chem. Phys.* **2004**, *4*, 2781–2804.
(21) Petters, S. S.; Petters, M. D. Surfactant Effect on Cloud Condensation Nuclei for Two-Component Internally Mixed Aerosols. *J. Geophys. Res. Atmos.* **2016**, *121*, 1878–1895.
(22) Prisle, N. L.; Raatikainen, T.; Laaksonen, A.; Bilde, M. Surfactants in Cloud Droplet Activation: Mixed Organic-Inorganic Particles. *Atmos. Chem. Phys.* **2010**, *10*, 5663–5683.
(23) Malila, J.; Prisle, N. L. A Monolayer Partitioning Scheme for Droplets of Surfactant Solutions. *J. Adv. Model. Earth Syst.* **2018**, doi: 10.1029/2018MS001456.
(24) Bzdek, B. R.; Power, R. M.; Simpson, S. H.; Reid, J. P.; Royall, C. P. Precise, Contactless Measurements of the Surface Tension of Picolitre Aerosol Droplets. *Chem. Sci.* **2016**, *7*, 274–285.
(25) Boyer, H. C.; Bzdek, B. R.; Reid, J. P.; Dutcher, C. S. Statistical Thermodynamic Model for Surface Tension of Organic and Inorganic Aqueous Mixtures. *J. Phys. Chem. A* **2017**, *121*, 198–205.
(26) Morris, H. S.; Grassian, V. H.; Tivanski, A. V. Humidity-Dependent Surface Tension Measurements of Individual Inorganic and Organic Submicrometre Liquid Particles. *Chem. Sci.* **2015**, *6*, 3242–3247.
(27) Lee, H. D.; Estillore, A. D.; Morris, H. S.; Ray, K. K.; Alejandro, A.; Grassian, V. H.; Tivanski, A. V. Direct Surface Tension Measurements of Individual Submicrometer Particles Using Atomic Force Microscopy. *J. Phys. Chem. A* **2017**, *121*, 8296–8305.
(28) Rayleigh, L. On the Capillary Phenomena of Jets. *Proc. R. Soc. London* **1879**, *29*, 71–97.
(29) Lamb, H. *Hydrodynamics, 6th Edition*; 1932.
(30) Chandrasekhar, S. The Oscillations of a Viscous Liquid Globe. *Proc. London Math. Soc.* **1959**, *s3-9*, 141–149.
(31) Bzdek, B. R.; Collard, L.; Sprittles, J. E.; Hudson, A. J.; Reid, J. P. Dynamic Measurements and Simulations of Airborne Picolitre-Droplet Coalescence in Holographic Optical Tweezers. *J. Chem. Phys.* **2016**, *145*, 054502.
(32) Endo, T.; Ishikawa, K.; Fukuyama, M.; Uraoka, M.; Ishizaka, S.; Hibara, A. Spherical Spontaneous Capillary-Wave Resonance on Optically Trapped Aerosol Droplet. *J. Phys. Chem. C* **2018**, *122*, 20684–20690.
(33) Staat, H. J. J.; van der Bos, A.; van den Berg, M.; Reinten, H.; Wijshoff, H.; Versluis, M.; Lohse, D. Ultrafast Imaging Method to Measure Surface Tension and Viscosity of Inkjet-Printed Droplets in Flight. *Exp. Fluids* **2017**, *58*, doi: 10.1007/s00348-016-2284-8.
(34) Ishiwata, T.; Sakai, K. Dynamic Surface Tension Measurement with Temporal Resolution on Microsecond Scale. *Appl. Phys. Express* **2014**, *7*, 077301.
(35) Hayakawa, D.; Hirano, T.; Mitani, S.; Sakai, K. Measurement of Surface Tension of Liquid Microdroplets through Observation of Droplet Collision. *Jpn. J. Appl. Phys.* **2017**, *56*, 7–9.
(36) Stückrad, B.; Hiller, W. J.; Kowalewski, T. A. Measurement of Dynamic Surface Tension by the Oscillating Droplet Method. *Exp. Fluids* **1993**, *15*, 332–340.
(37) Yang, L.; Kazmierski, B. K.; Hoath, S. D.; Jung, S.; Hsiao, W. K.; Wang, Y.; Berson, A.; Harlen, O.; Kapur, N.; Bain, C. D. Determination of Dynamic Surface Tension and Viscosity of Non-Newtonian Fluids from Drop Oscillations. *Phys. Fluids* **2014**, *26*, 113103.
(38) Hoath, S. D.; Hsiao, W. K.; Martin, G. D.; Jung, S.; Butler, S. A.; Morrison, N. F.; Harlen, O. G.; Yang, L. S.; Bain, C. D.; Hutchings, I. M. Oscillations of Aqueous PEDOT:PSS Fluid Droplets and the Properties of Complex Fluids in Drop-on-Demand Inkjet Printing. *J. Nonnewton. Fluid Mech.* **2015**, *223*, 28–36.
(39) Vaughn, B. S.; Tracey, P. J.; Trevitt, A. J. Drop-on-Demand Microdroplet Generation: A

Very Stable Platform for Single-Droplet Experimentation. *RSC Adv.* **2016**, *6*, 60215–60222.
(40) Jacobs, M. I.; Davies, J. F.; Lee, L.; Davis, R. D.; Houle, F.; Wilson, K. R. Exploring Chemistry in Microcompartments Using Guided Droplet Collisions in a Branched Quadrupole Trap Coupled to a Single Droplet, Paper Spray Mass Spectrometer. *Anal. Chem.* **2017**, *89*, 12511–12519.
(41) Kohno, J. Y.; Kobayashi, M.; Suzuki, T. Protrusion Formation during the Collisional Process of Ethanol and Water Droplets: Capillary Wave Propagation on the Water Droplet. *Chem. Phys. Lett.* **2013**, *578*, 15–20.
(42) Power, R. M.; Simpson, S. H.; Reid, J. P.; Hudson, A. J. The Transition from Liquid to Solid-like Behaviour in Ultrahigh Viscosity Aerosol Particles. *Chem. Sci.* **2013**, *4*, 2597–2604.
(43) Symes, R.; Sayer, R. M.; Reid, J. P. Cavity Enhanced Droplet Spectroscopy: Principles, Perspectives and Prospects. *Phys. Chem. Chem. Phys.* **2004**, *6*, 474–487.
(44) Preston, T. C.; Reid, J. P. Accurate and Efficient Determination of the Radius, Refractive Index, and Dispersion of Weakly Absorbing Spherical Particle Using Whispering Gallery Modes. *J. Opt. Soc. Am. B* **2013**, *30*, 2113–2122.
(45) Wexler, A. S.; Dutcher, C. S. Statistical Mechanics of Multilayer Sorption: Surface Tension. *J. Phys. Chem. Lett.* **2013**, *4*, 1723–1726.
(46) Boyer, H. C.; Dutcher, C. S. Atmospheric Aqueous Aerosol Surface Tensions: Isotherm-Based Modeling and Biphasic Microfluidic Measurements. *J. Phys. Chem. A* **2017**, *121*, 4733–4742.

FIGURES

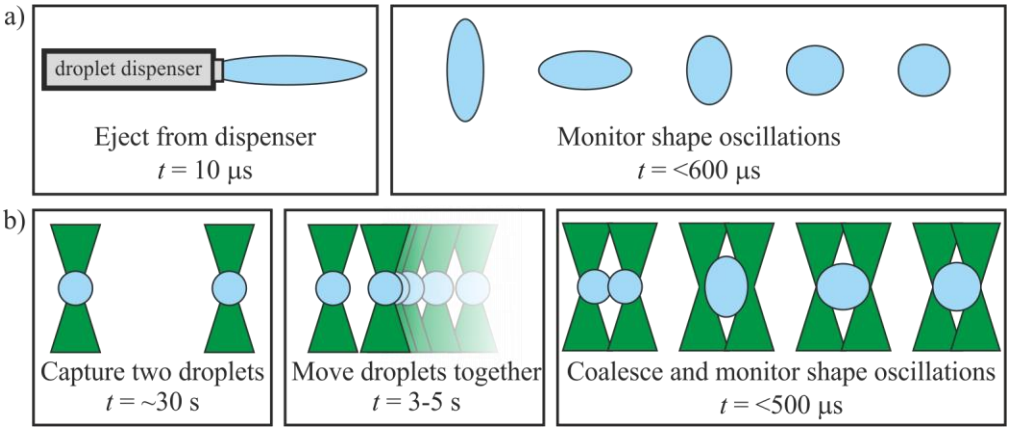

Figure 1. Pictorial description of the two experimental approaches used to measure the surface tension of picoliter volume droplets. For both approaches, surface tension is retrieved from oscillations in droplet shape. a) The microdroplet dispenser approach produces droplets with surface age <1 ms. b) The holographic optical tweezers approach measures the surface tension of droplets with much longer surface ages.

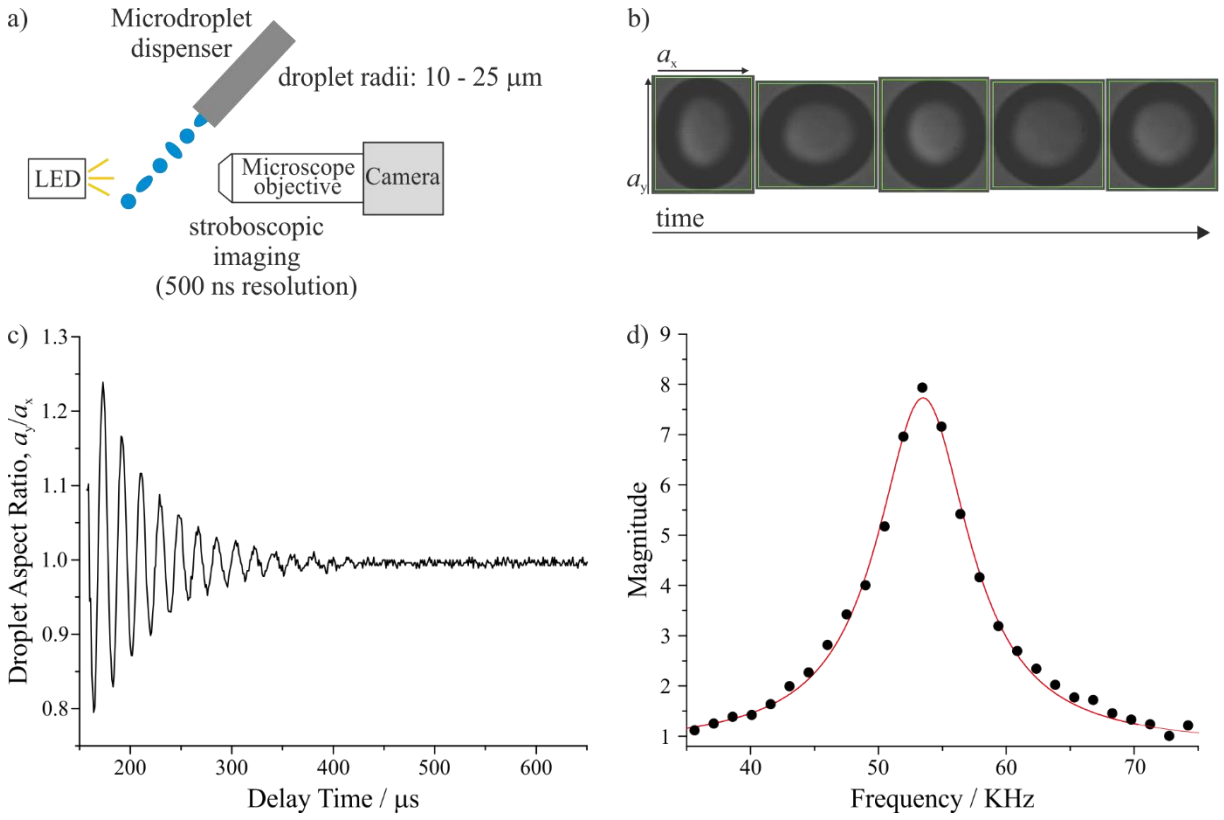

Figure 2. a) Schematic of the microdroplet dispenser approach to study the surface tension of droplets with fresh surfaces. Droplets are ejected from the dispenser and stroboscopically imaged. b) After ejection from the microdroplet dispenser, droplets relax to spherical shape by undergoing damped shape oscillations. c) The droplet aspect ratio is plotted against delay time to visualize the oscillations. d) A Lorentzian fit to the Fast Fourier Transform of the droplet aspect ratio plot gives the frequency of the oscillations, which is used to retrieve surface tension.

548

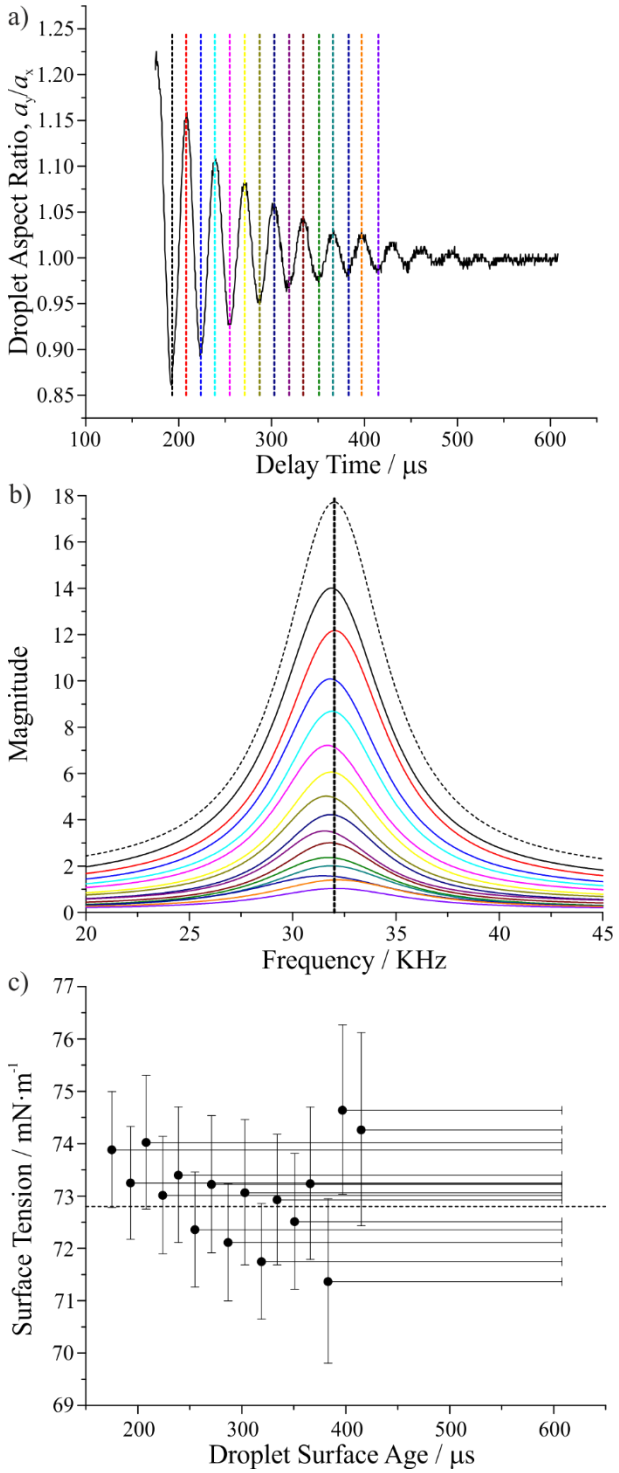

549

550 **Figure 3.** Analysis of a 24 µm radius pure water droplet. a) Droplet aspect ratio plotted against

551 delay time. The data to the right of each vertical dotted line underwent a separate Fast Fourier

552 Transform and corresponds to individual traces in part b). b) Lorentzian fits to Fast Fourier

Transforms for various portions of the droplet aspect ratio plot in part a). c) Surface tension of the water droplet plotted against surface age. The x-uncertainty indicates the droplet surface age range over which the droplet aspect ratio plot (a) was Fast Fourier Transformed. The dotted line shows the expected value.

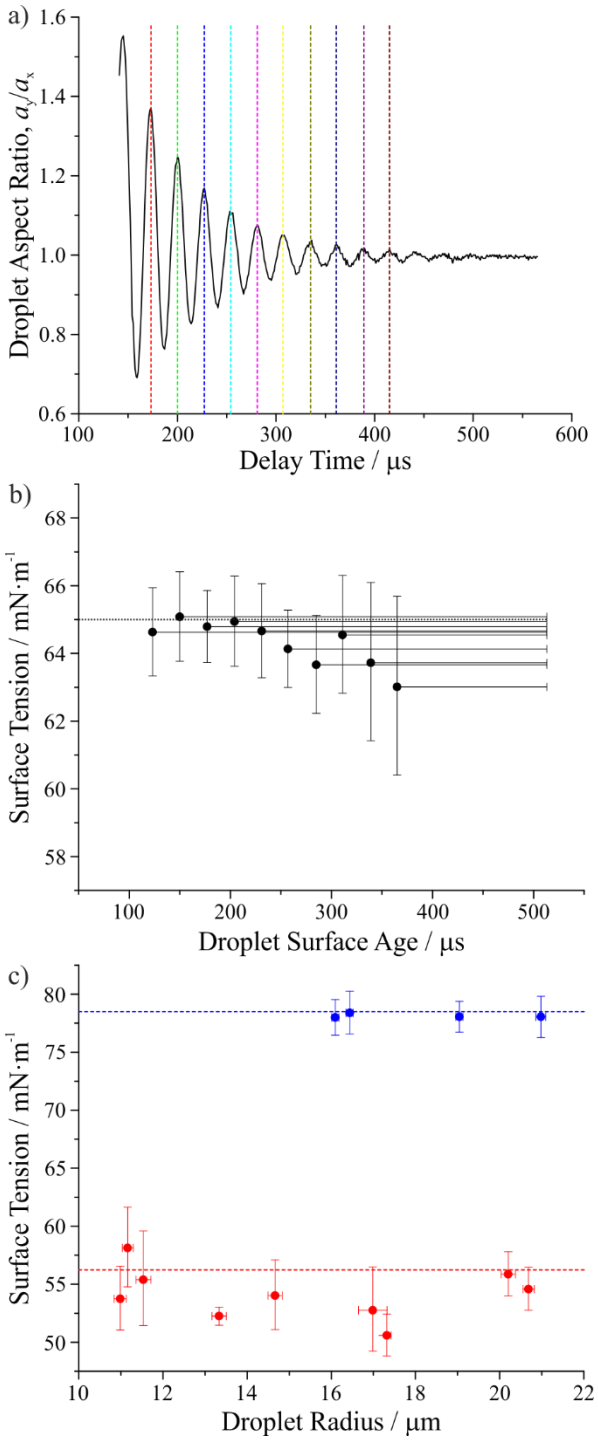

558

559 **Figure 4.** a) Droplet aspect ratio vs. delay time for a 21 µm radius glutaric acid-water droplet with

560 0.01 solute mole fraction. These data were used to obtain the surface tension values plotted in b).

561 The data to the right of each vertical dotted line underwent a separate Fast Fourier Transform and

562 correspond to individual data points in b), showing no dependence of glutaric acid surface tension
563 as a function of droplet surface age. The x-uncertainty in b) indicates the portion of the droplet
564 aspect ratio plot that was Fast Fourier Transformed. c) Glutaric acid-water droplets (0.090 mole
565 fraction, red symbols) and sodium chloride-water droplets (0.062 mole fraction, blue symbols)
566 whose surface tensions were studied as a function of droplet radius. Dotted lines show surface
567 tensions from comparable bulk measurements.
568

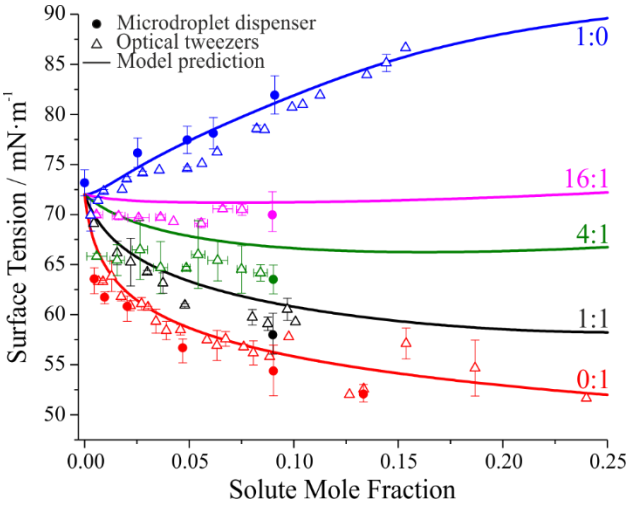

569

570 **Figure 5.** Surface tension plotted against solute mole fraction ($x_{NaCl} + x_{GA}$) for several different
571 aqueous sodium chloride:glutaric acid mass ratio systems. Closed symbols represent the
572 microdroplet dispenser measurements. Open triangles represent holographic optical tweezers
573 measurements. Solid lines represent statistical thermodynamic model predictions.

574

575 **TOC GRAPHIC**

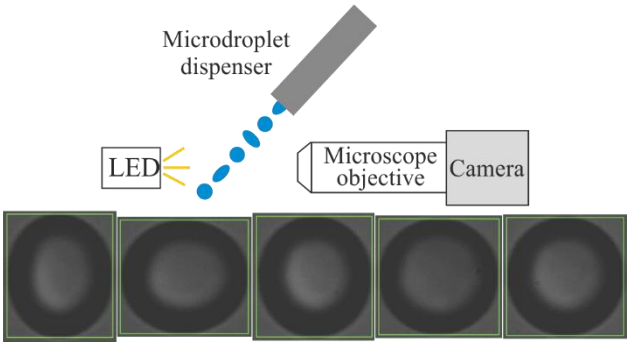

576

577

Author Biography

Bryan R. Bzdek is a NERC independent research fellow at the University of Bristol. He earned a B.S. degree in chemistry at Bucknell University (2008) and performed undergraduate research with Molly McGuire. He earned a Ph.D. degree in chemistry with Murray Johnston at the University of Delaware (2014). He performed postdoctoral research with Jonathan Reid at Bristol (2014–2017) before starting his independent career at Bristol. His interests include development of single particle approaches to study aerosol physicochemical properties. His work in aerosol science has been acknowledged by the American Association for Aerosol Research through the Sheldon K. Friedlander Award (2017).